H, $CH_2C{=}Cr$), 4.00 (t, J = 6.5 Hz, 2 H, CH_2S); IR (hexane) ν_{CO} 2061 (w), 1959 (s, b) cm^{-1}; exact mass 277.9331 (calcd for $C_9H_5O_5SCr$ 277.9340); MS [m/e (%)] 278 (28), 194 (15) M – 3CO, 178 (12), 166 (40) M – 4CO, 162 (23), 138 (100) M – 5CO, 119 (23), 111 (27), 110 (46), 105 (35), 102 (42), 97 (27), 86 (29), 85 (61), 83 (35), 81 (31), 79 (35), 69 (46), 52 (96).

Reaction of the Anion of 1 with Acetyl Chloride. *n*-BuLi (0.31 mL, 1.65 M, 0.51 mmol) was added to **1** (125 mg, 0.48 mmol) in 10 mL of THF at –78 °C. After 5 min, acetyl chloride (60 μL, 0.84 mmol) was injected followed by warming to 25 °C and stirring for 50 min. Removal of solvent and preparative TLC (1:1 hexane–ether) gave **1** (49 mg, 39% recovery, R_f 0.35) and **22** (70 mg, 43%, R_f 0.25). NMR indicated that **22** was a 1:1 mixture of the *Z* and *E* isomers; the mixture was isolated as a red solid and could not be separated by preparative TLC: NMR (CS_2) δ 2.17 (s, $CH_3C{=}O$), 2.24 (bs, $CH_3C{=}C$), 2.35 (s, $CH_3C{=}O$), 2.82 (s, $CH_3C{=}C$), 2.66 (m, $CH_2C{=}C$ of both isomers), 4.70 (two overlapping triplets, J = 7 Hz, CH_2O of both isomers); IR (hexane) ν_{CO} 2058 (m), 1985 (m), 1950 (sh, s), 1944 (s), C=O (enol acetate) 1775 cm^{-1}; exact mass 345.9773 (calcd for $C_{13}H_{10}O_8Cr$ 345.9779); MS [m/e (%)] 346 (14), 234 (19) M – 4CO, 206 (34) M – 5CO, 178 (65), 176 (21), 163 (50), 150 (50), 139 (19), 135 (15), 128 (69), 121 (18), 113 (35), 111 (32), 82 (14), 80 (19), 69 (34), 67 (31), 52 (100).

Reaction of the Anion of 8 with Acetyl Chloride. *n*-BuLi (0.62 mL, 1.61 M, 1.0 mmol) was added to **8** (250 mg, 0.91 mmol) in 15 mL of THF at –78 °C. Acetyl chloride (78 μL, 1.1 mmol) was injected followed by stirring for 30 min at –78 °C and 30 min at 25 °C. Preparative TLC (1:1 pentane–ether) gave **8** (35 mg, 14% recovery, R_f 0.30) and **24** (189 mg, 65%, R_f 0.08) as a yellow solid: mp 59–61 °C; NMR ($CDCl_3$) δ 1.75 (s, 3 H, CH_3), 1.7–2 (m, 1 diastereotopic H of CH_2CH_2O), 2.2–2.5 (m, 1 diastereotopic H of CH_2CH_2O), 2.32 (s, 3 H, $CH_3C{=}O$), 5.01 (m, 2 H, CH_2O); IR (hexane) ν_{CO} 2064 (w), 1993 (w), 1962 (s), 1953 (s), 1926 (m) cm^{-1}; exact mass 317.9815 (calcd for $C_{12}H_{10}O_7Cr$ 317.9830); MS [m/e (%)] 318 (1) M^+, 290 (8) M – 1CO, 262(3) M – 2CO, 234 (5) M – 3CO, 206 (11) M – 4CO, 178 (21) M – 5CO, 126 (12), 123 (12), 111 (5), 83 (6), 80 (6), 55 (7), 52 (7), 43 (15), 28 (100).

Reaction of the Anion of 1 with Bromine. *n*-BuLi (0.28 mL, 1.50 M, 0.42 mmol) was added to **1** (100 mg, 0.38 mmol) in 10 mL of THF at –78 °C. Bromine (24 μL, 0.42 mmol) was added dropwise and the reaction was stirred 5 min at –78 °C and 10 min at 25 °C. Preparative TLC (2:1 hexane–ether) gave α-bromo-γ-butyrolactone (10 mg, 16%, R_f 0.10), which was identified by comparison of its IR spectrum with that of an authentic sample, and **25** (71 mg, 55%, R_f = 0.25) as a red-orange oil: NMR (CS_2) δ 2.38 (m, 2 H, CH_2CH_2O), 4.88 (m, 2 H, CH_2O), 5.50 (m, 1 H, CHBr); IR (hexane) ν_{CO} 2068 (w), 1997 (w), 1969 (s), 1960 (s), 1946 (s) cm^{-1}; exact mass 339.8662 (calcd for $C_9H_5BrO_6Cr$ 339.8673); MS [m/e (%)] 340 (3) M^+, 312 (0.5) M – 1CO, 256 (1) M – 3CO, 228 (3) M – 4CO, 200 (4) M – 5CO, 170 (4), 149 (5), 138 (5), 121 (6), 120 (4), 97 (5), 91 (8), 82 (93), 81 (31), 80 (100), 69 (6), 52 (18).

Acknowledgment. This research was supported by the National Science Foundation.

Registry No. **1**, 54040-15-2; **3**, 64082-32-2; **4**, 64082-31-1; **8**, 54040-17-4; **9**, 64082-30-0; **13**, diastereomer 1, 64129-90-4; **13**, diastereomer 2, 64082-29-7; **14**, diastereomer 1, 64130-28-5; **14**, diastereomer 2, 64082-28-6; **15**, 64082-27-5; **16**, diastereomer 1, 64129-89-1; **16**, diastereomer 2, 64082-26-4; **11**, 61989-11-5; **10**, 64082-25-3; **17**, 20540-69-6; **18**, 64091-77-6; **19**, 64091-76-5; **20**, 64091-75-4; **21**, 64103-52-2; **22** (*Z* isomer), 64130-26-3; **22** (*E* isomer), 64091-74-3; **24**, 64091-86-7; **25**, 64091-85-6; methyl vinyl ketone, 78-94-4; *trans*-$CH_3CH{=}CHCOCH_3$, 3102-33-8; *trans*-$C_6H_5CH{=}CHCOCH_3$, 1896-62-4; 2-cyclohexen-1-one, 930-68-7; *trans*-$CH_3CH{=}CHCO_2CH_3$, 623-43-8; benzyl bromide, 100-39-0; methyl acrylate, 96-33-3; ethylene sulfide, 420-12-2; acetyl chloride, 75-36-5; Br_2, 7726-95-6; α-bromo-α-butyrolactone, 5061-21-2.

References and Notes

(1) C. P. Casey in "Transition Metal Organometallics in Organic Synthesis", Vol. I, H. Alper, Ed., Academic Press, New York, N.Y., 1976, Chapter 3.
(2) K. H. Dotz, *Naturwissenschaften*, **62**, 365 (1975).
(3) C. P. Casey, R. A. Boggs, and R. L. Anderson, *J. Am. Chem. Soc.*, **94**, 8947 (1972).
(4) C. P. Casey and R. L. Anderson, *J. Organomet. Chem.*, **73**, C28 (1974).
(5) C. P. Casey and W. R. Brunsvold, *J. Organomet. Chem.*, **102**, 175 (1975).
(6) C. P. Casey, R. A. Boggs, D. F. Marten, and J. C. Calabrese, *J. Chem. Soc., Chem. Commun.*, 243 (1973).
(7) C. P. Casey and W. R. Brunsvold, *J. Organomet. Chem.*, **118**, 309 (1976).
(8) C. G. Kreiter, *Angew. Chem., Int. Ed. Engl.*, **7**, 390 (1968).
(9) C. P. Casey and R. L. Anderson, *J. Am. Chem. Soc.*, **96**, 1230 (1974).
(10) C. P. Casey and W. R. Brunsvold, *Inorg. Chem.*, **16**, 391 (1977).
(11) C. P. Casey and W. R. Brunsvold, *J. Organomet. Chem.*, **77**, 345 (1974).
(12) E. O. Fischer and F. R. Kreissl, *J. Organomet. Chem.*, **35**, C47 (1972).
(13) F. R. Kreissl, E. O. Fischer, and C. G. Kreiter, *J. Organomet. Chem.*, **57**, C9 (1973).
(14) C. P. Casey, *Chem. Commun.*, 1220 (1970).
(15) E. D. Bergmann, D. Ginsburg, and R. Pappo, *Org. React.*, **10**, 179 (1959).

Contribution from Erindale College and The Lash Miller Chemistry Laboratory, University of Toronto, Toronto, Ontario, Canada

Metal Atom–Metal Cluster Chemistry. 1. Alkane Matrices

WERNER E. KLOTZBÜCHER, STEVEN A. MITCHELL, and GEOFFREY A. OZIN*†

Received May 19, 1977 AIC70366+

The optical spectra (200–700 nm) of vanadium atoms isolated in a series of normal, branched, and cyclic alkanes have been recorded over a temperature range between 10 K and approximately half the melting point of the matrix material. The atomic spectra are less well defined in alkane matrices than in argon matrices, but matrix-induced frequency shifts from gas-phase values are smaller and they tend to decrease with increasing chain length of the normal alkane matrix material. The temperature at which metal atom diffusion becomes appreciable in these matrices, during controlled matrix warm-up, correlates roughly with one-third of the melting point of the matrix material. The influence of the matrix material on the extent to which divanadium forms on the surface of the matrix during deposition is considered in terms of a steady-state model for the deposition process. Under similar deposition conditions, alkane matrices are more efficient than argon matrices for isolation of atoms over diatomic and higher polyatomic molecules, and the isolation efficiency increases with increasing chain length of the normal alkane matrix material.

Introduction

In recent years there has been much interest expressed in the effects of low-temperature matrix environments on the optical spectra of metal atoms. These effects, which often result in substantial differences between gas-phase and matrix spectra, include frequency shifts from gas-phase values and splitting of single gas-phase lines.[1] Matrix-induced changes in atomic optical spectra are of particular interest in so far as they relate to studies in the area of metal atom matrix chemistry. As ultraviolet–visible spectroscopy is of basic importance in this area, it is desirable to clearly establish atomic spectra in different matrix environments. Atomic spectral features may then be more readily distinguished from

† Sherman-Fairchild Distinguished Scholar, 1977, California Institute of Technology, Pasadena, Calif.

molecular absorptions arising from the products of cocondensation reactions.

Although noble gases are most commonly used in matrix isolation studies, some workers have reported atomic optical spectra in hydrocarbon matrices. Duley[2] has reported the optical spectra of several metals isolated in low-temperature aromatic and paraffin matrices. The isolation of titanium atoms in cyclohexane matrices at 55 K was reported to result in an optical spectrum less complex than that observed for argon matrices, with smaller shifts of the atomic absorptions from gas-phase frequencies.[2a] Optical spectra obtained for manganese atoms isolated in benzene matrices between 55 and 135 K have also been reported by Duley.[2b] This system was found to be characterized by high thermal stability, with little or no diffusion of the isolated atoms occurring during warming of the matrix.

The high melting points of many hydrocarbons, relative to the melting points of the noble gases, suggest that hydrocarbon matrices may be useful variable-temperature reaction media for observing metal atom cryochemical processes over a much wider temperature range than is presently possible with noble gas matrices. In this way, kinetic impediments to product formation in the noble gases may be overcome by employing higher temperature deposition and annealing conditions in alkane supports. In this context, we believe that greater control of the embryonic stages of naked metal cluster agglomeration reactions in alkane matrices compared to the noble gases is an intriguing possibility and worthy of investigation.

The potential for assessing the thermal stability of the products of low-temperature cocondensation reactions from 10 to 300 K is also of particular interest.

Because hydrocarbon matrices have intense absorptions in the infrared region, the usefulness of the more complex hydrocarbon matrices is likely to be largely restricted to the optically transparent ultraviolet–visible spectral region. It is of interest, therefore, to investigate the optical properties of transition-metal atoms and small, well-defined naked metal clusters isolated in a wide variety of hydrocarbon matrices and the dependence of these properties on the temperature of the matrix. Hydrocarbon matrices may also be useful in macroscale synthetic and catalytic applications. For example, the use of alkanes for low-temperature (−196 °C) cocondensation with nickel and magnesium atoms has been reported by Klabunde.[3] In the case of nickel, normal hexane was found to be useful as a solvent for the low-temperature preparation of small nickel aggregates which were subsequently used as a hydrogenation catalyst for benzene and norbornene.[3a] Cocondensation of magnesium atoms with THF or normal hexane resulted in the formation of a magnesium slurry which was very active for Grignard reagent preparation.[3b]

The low-temperature preparation of metal aggregate dispersions in solid or liquid hydrocarbons is a technique with some very interesting potential applications. Colloidal dispersions of varying particle size may be useful for the preparation of supported catalysts and for studies of heterogeneous catalysis in hydrocarbon solvents. We believe that matrix scale spectroscopic studies of the diffusion and aggregation properties of metal atoms in hydrocarbon matrices can provide a fundamental starting point for future research in this area. Of particular interest is the influence of the matrix material and deposition conditions on the distribution of metal between atoms and polyatomic species. The initial distribution of metal among these species and the subsequent warm-up conditions are expected to be of importance in determining the final size distribution and properties of the resulting metal aggregate dispersion.

In view of our detailed spectroscopic studies of V atoms and V_2 molecules in noble gas matrices,[4a] we have chosen in this paper to investigate the optical spectra of vanadium atoms and diatomic vanadium molecules in a variety of alkane matrices between 10 and approximately 80 K. Some observations regarding the influence of the matrix material on the diffusion properties of vanadium atoms on the surface of the matrix during deposition and within the matrix during controlled warm-up are also reported.

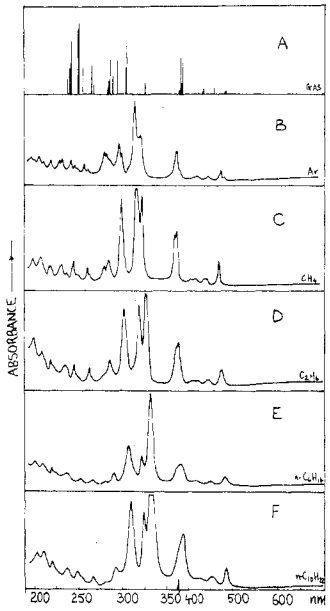

Figure 1. (A) Gas-phase atomic spectrum of vanadium (ref 7) compared to isolated atomic vanadium in (B) Ar, (C) CH_4, (D) C_2H_6, (E) n-C_6H_{14}, and (F) n-$C_{10}H_{22}$ matrices at 10–12 K.

Experimental Section

Monatomic V was generated by directly heating a thin vanadium filament (0.010 in.). The vanadium metal (99.99%) was supplied by A. D. McKay, New York, N.Y. Research grade Ar, CH_4, C_2H_6, C_3H_8, and n-C_4H_{10} were supplied by Matheson of Canada. High-purity liquid alkanes were obtained from the Aldrich Chemical Co., and the purity was confirmed by chromatographic analysis on a Poropak Q column. Dissolved gases were removed from these liquids by repeated freeze, pump, thaw cycles. Gaseous samples of alkanes with vapor pressures exceeding 50 Torr were prepared by evaporation of the liquid into gas bulbs. Liquid samples were employed for the low vapor pressure alkanes, the vapor above the liquid being used for condensation onto the optical window. The furnace used for evaporation of the vanadium has been described previously.[5] The rate of metal atom deposition was continuously monitored using a quartz crystal microbalance.[5] To obtain quantitative data for the V/hydrocarbon cocondensations, it was necessary to calibrate carefully the rate of deposition of both metal and each hydrocarbon onto the sample window. Matrices were deposited on a NaCl plate cooled to 10–12 K by means of an Air Products Displex closed-cycle helium refrigerator. The temperature of the optical plate was measured using a gold–0.07 atom % iron vs. chromel thermocouple. UV–visible spectra were recorded on a standard Unicam SP 8000 instrument in the range 200–700 nm.

Optical Spectra of Vanadium Atoms in Alkane Matrices

The optical spectra of vanadium atoms in some representative matrices, which were obtained under dilute conditions (V:alkane $\simeq$ 1:10^3) at 10–12 K, are shown in Figure 1 together with the gas-phase spectrum. The qualitative features of the spectra are reproduced quite well in each matrix considered and these correlate reasonably well with the gas-phase spectrum.

For the spectra obtained in argon and methane matrices, the line widths appear to be comparable. In ethane matrices the lines are somewhat broader and some differences are observed in the structures of the higher energy absorptions.

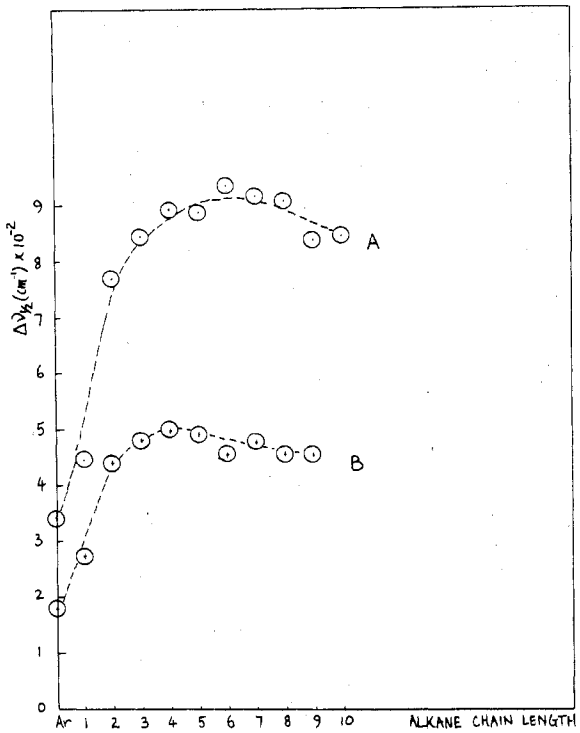

Figure 2. Graphical representation of the variation of bandwidths at half-heights (cm^{-1}) for two well-resolved absorptions of atomic vanadium, (A) 296.7-nm Ar band and (B) 472.5-nm Ar band, in C_nH_{2n+2} matrices at 10–12 K (where n = 1–10).

Table I. Bandwidths at Half-Height[a] for Two Well-Resolved Absorptions of Atomic Vanadium in C_nH_{2n+2} Matrices at 10–12 K (Where n = 1–10)

		Bandwidths		
	$\Delta\nu_{1/2}^{C_nH_{2n+2}}/\Delta\nu_{1/2}^{Ar}$	296.7 nm (Ar)	472.5 nm (Ar)	$\Delta\nu_{1/2}^{C_nH_{2n+2}}/\Delta\nu_{1/2}^{Ar}$
Ar	1.000	341.3	179.5	1.000
CH_4	1.305	445.3	271.6	1.513
C_2H_6	2.242	765.1	439.6	2.449
C_3H_8	2.472	843.6	480.5	2.677
C_4H_{10}	2.609	890.4	498.7	2.778
C_5H_{12}	2.598	886.8	494.6	2.755
C_6H_{14}	2.735	933.3	453.7	2.528
C_7H_{16}	2.679	914.4	476.5	2.655
C_8H_{18}	2.659	907.5	455.5	2.538
C_9H_{20}	2.447	835.3	455.6	2.538
$C_{10}H_{22}$	2.471	843.3	442.5	2.465

[a] Units in cm^{-1}.

These differences in the appearance of the high-energy region of the spectrum may be due to multiple trapping site effects or they may be caused by varying shifts of closely spaced lines, which result in varying degrees of overlap in different matrices. The strong absorptions near 315 nm in argon ($3d^34s^2 \rightarrow 3d^34s^14p^1$) show a similar intensity ratio in methane, but this ratio is reversed in ethane and in the other alkanes. Some dependence on the deposition conditions has been observed for the intensity ratio of these lines in CH_4. Table I and Figure 2 show the observed variation with matrix material, of the bandwidths at half-height, of two representative and reasonably well-resolved atomic vanadium absorption bands (denoted 296.7 nm Ar and 472 nm Ar). On passing from Ar to CH_4 to higher straight chain alkanes, the line widths (cm^{-1}) gradually increase up to C_4H_{10}/C_5H_{12} and then remain roughly constant up to the last member of our experimental series, decane. Note that the relative bandwidths for these two absorptions with respect to the corresponding Ar lines

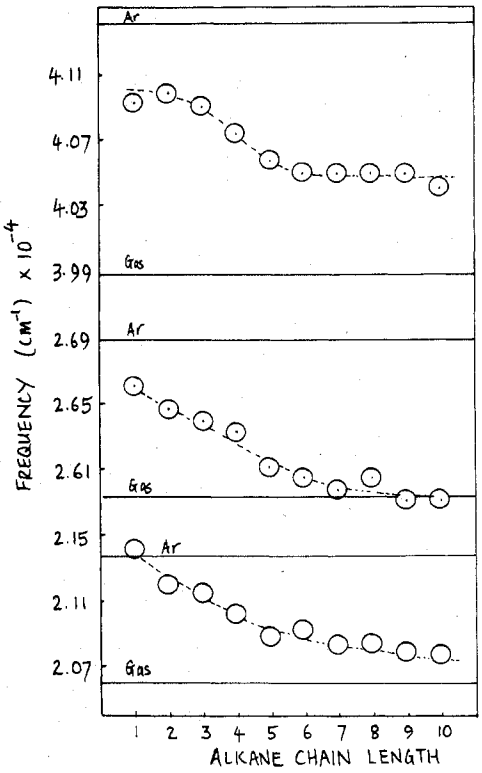

Figure 3. Frequencies of three representative vanadium atom absorptions in different straight chain C_nH_{2n+2} matrices (where n = 1–10) compared to gas-phase and argon isolated atomic vanadium.

($\Delta\nu_{1/2}^{C_nH_{2n+2}}/\Delta\nu_{1/2}^{Ar}$ in Table I) show a roughly parallel behavior with increasing chain length. The increasing widths of these atomic lines may be a reflection of a greater diversity in the local environments of atoms trapped in the higher alkanes (that is, inhomogeneous line broadening rather than induced dipole–dipole crystal field type effects). Finally on the subject of bandwidths, we note that for a group of geometrical isomers such as *n*-hexane, 2-methylpentane, and 2,3-dimethylbutane and also for cyclohexane, the bandwidths of the two representative atomic vanadium absorptions remain essentially invariant.

Aside from the differences mentioned above and the shifts in the positions of the absorptions discussed below, the spectra are very similar for all of the matrices considered, and one-to-one correlations between the argon matrix spectrum and the alkane matrix spectra are possible for most of the absorptions. We have previously reported a tentative correlation between the gas-phase and argon matrix spectra of vanadium atoms.[4a] However, because of the large number of atomic absorptions observed and because of the large apparent shifts in the positions of these lines, some of these assignments are uncertain, as is further discussed below.

The effect of the alkane matrices on the positions of the atomic absorptions, relative to corresponding absorptions in argon, is generally a shift to lower energy. In most cases, as is illustrated in Figure 3 for three representative absorptions, the observed frequency shift varies monotonically with the chain length of the normal alkane matrix material. The observed frequency shifts for the strongest absorption features of the optical spectra are listed in Table II for argon, methane, pentane, and decane matrices.

Figure 3 and Table II show that in alkane matrices most of the atomic absorptions undergo substantial shifts to lower energy from their positions in argon matrices and that the shifts (like the bandwidths) appear to reach a *limiting* value in decane matrices. The matrix atomic spectra show only small frequency shifts when different *geometrical isomers* of a parent

Table II. Positions of Vanadium Atom Lines and Frequency Shifts in Various Matrices

λ(argon), nm	ν(argon), cm^{-1}	λ(CH_4), nm	ν(CH_4), cm^{-1}	ν(argon − CH_4), cm^{-1}	λ(C_5H_{12}), nm	ν(C_5H_{12}) cm^{-1}	ν(argon − C_5H_{12}), cm^{-1}	λ($C_{10}H_{22}$), nm	ν($C_{10}H_{22}$), cm^{-1}	ν(argon − $C_{10}H_{22}$), cm^{-1}
468	21 367	468	21 367	0	480	20 833	534	481.5	20 768	599
440	22 727	434	23 041	−314	449	22 272	455	452	22 124	603
372	26 881	375	26 667	214	383	26 110	771	386	25 907	974
320	31 250	321.5	31 104	146	329	30 395	855	330	30 303	947
313	31 948	315.5	31 696	252	322	31 056	892	323	30 960	988
296	33 783	298.5	33 501	282	306.5	32 626	1156	308.2	32 446	1337
281	35 587	283.5	35 273	314	288	34 722	865	291.5	34 305	1282
256.5	38 986	259	38 601	376	263	38 022	963	264	37 879	1107
241.5	41 407	244.5	40 900	507	246.5	40 568	839	247.5	40 404	1003
231.5	43 196	230.5	43 384	−188	236	42 313	823	235	42 553	643
219	45 662	216.5	46 189	−527	219	45 662	0	219	45 662	0
205.5	48 661	207	48 309	352	209.5	47 733	928	209	47 847	814
198	50 505	197.5	50 633	−128	200.5	49 875	630	201	49 751	754

Table III. Frequencies of Three Representative Absorption Bands in Different "Geometric Isomer Matrices" C_nH_{2n+2} (Where n = 5–7; Cyclic Analogues Are also Included for Comparison Purposes)

Matrix	Band I, nm	Band II, nm	Band III, nm
Pentane	480	383	247
Cyclopentane	475	383	247
2-Methylbutane	481	383	247
Hexane	479	384	247
Cyclohexane	479	385	247
2-Methylpentane	481	385	247
2,3-Dimethylbutane	482	385	247
Heptane	481	385	247
Cycloheptane	477	384	247
2-Methylhexane	480	384	247
2,3-Dimethylpentane	482	383	247

alkane are used. Some examples of this are given in Table III and Figure 4.

The matrix/gas-phase correlations indicated in Figure 3 should be regarded only as tentative assignments. It is interesting to note, however, that a reasonable correlation of the gas phase and decane matrix spectra is possible for which all of the strong absorptions show the same qualitative behavior as the three absorptions illustrated in Figure 3. Such a correlation is given in Table IV.

The trend toward decreasing blue shift with increasing alkane chain length, as illustrated in Figure 3, may be rationalized in a very simple way. With increasing size of the molecules of the matrix material, the trapping sites become larger so that guest–host repulsive interactions are reduced and the atomic spectra begin to resemble more closely that which is observed in the gas phase. If this interpretation is correct, then alkane matrices, and decane in particular, may be generally useful in correlating matrix and gas-phase atomic spectra. Therefore the opportunity of extending the approach

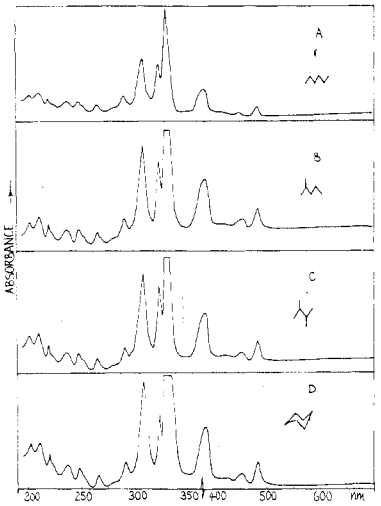

Figure 4. Ultraviolet–visible spectra of atomic vanadium in various geometrical isomer hexane matrices: (A) *n*-hexane, (B) 2-methylpentane, (C) 2,3-dimethylbutane, and for comparison (D) cyclohexane.

to transition-metal clusters and cluster complexes becomes an attractive proposition. Note, however, that because of the glassy and generally poorly defined nature of alkane matrices, the actual definition of the "size" of a lattice trapping site becomes a tenuous proposition and our rationale of the dependence of atomic spectral shifts as a function of alkane chain length can only be regarded as speculation until crystal structure data for low-temperature alkane films become available.

Diffusion of Vanadium Atoms in Argon and Alkane Matrices

The behavior of atomic optical spectra during controlled matrix warm-up studies gives an indication of the bulk diffusion and aggregation properties of matrix-isolated atoms.

Table IV. Band Assignments and Matrix Shifts for Vanadium in Argon and Decane Matrices

ν(gas), cm^{-1}	λ(argon), nm	ν(argon), cm^{-1}	ν(argon) − ν(gas), cm^{-1}	λ($C_{10}H_{22}$) nm	ν($C_{10}H_{22}$) cm^{-1}	ν($C_{10}H_{22}$) − ν(gas), cm^{-1}
20 606	468	21 367	761	481.5	20 768	162
21 841	440	22 727	886	452	22 124	283
25 931	372	26 881	950	386	25 907	−24
30 636	320	31 250	614	330	30 303	−333
30 636	313	31 948	1312	323	30 960	324
32 738	296	33 783	1045	308.2	32 446	−292
34 477	281	35 587	1110	291.5	34 305	−172
37 757	256.5	38 986	1229	264	37 879	121
39 878	241.5	41 407	1529	247.5	40 404	526
39 935	231.5	43 196	3261	235	42 553	2618
41 389	219	45 662	4273	219	45 662	4273
41 655	205.5	48 661	7006	209	47 847	6192
41 928	198	50 505	8577	201	49 751	7823

Table V. Diffusion Properties of Vanadium Atoms in Acyclic and Cyclic Alkane Supports (Some Matrix Properties Are Included)

Matrix material	T_{mp}, K	$^1/_3 T_{mp}$, K	T_{diff},[a] K	VP_{298}, Torr	ΔH_{fus}, kJ mol^{-1}	r/C[b]
Ar	83.0	27.7	36		1.21	128
CH_4	90.7	30.2	33		0.93	303
C_2H_6	89.9	30.0	28		2.85	31
C_3H_8	91.5	30.5	40		3.52	22
n-C_4H_{10}	134.8	44.9	44		4.65	44
n-C_5H_{10}	143.5	47.8	50	450.8	8.40	16
n-C_6H_{14}	177.9	59.3		37.9	13.05	12
n-C_7H_{16}	182.6	60.9	63	41.7	14.13	11
n-C_8H_{18}	216.4	72.1		13.6	20.61	7
n-C_9H_{20}	219.7	73.2		4.6	15.44	14
n-$C_{10}H_{22}$	243.1	81.0		1.8	28.72	5
Cyclopropane	145.0	48.6	22		5.43	40
Cyclopentane	179.3	59.8	46	321.2	0.61	5640
Cyclohexane	279.7	93.2		83.2	2.63	907
Cycloheptane	261.2	87.1	65			
Cyclooctane	287.5	95.8				
2-Methylbutane	113.2	37.7	57	631.2	5.14	21
2,3-Dimethylbutane	144.1	48.0	31	206.8	0.80	1810
2-Methylpentane	119.4	39.8	38	207.0	6.26	17
2,3-Dimethylpentane				65.3		
2-Methylhexane	155.2	51.7	55	57.9	8.85	18

[a] Temperature at which V atomic absorptions decrease by 10% during matrix warm-up. (Some variations in these temperatures are anticipated because of slightly different V/alkane concentration conditions and baseline uncertainties.) [b] Immobilization rate constant (see text).

Such studies have been carried out for the matrices indicated in Table V. Each matrix appeared to be unreactive toward CH and CC bond cleavage with vanadium atoms over the temperature range examined, but bulk diffusion and pronounced aggregation of the isolated atoms caused a steady decrease in the atomic absorptions upon warming of the matrices. No well-defined absorptions attributable to small V_n clusters were observed during these warm-up scans, although changes in the optical properties of the matrices often caused unpredictable changes in the baseline. For this reason, quantitative comparisons of atomic absorptions at different temperatures were difficult. In some cases annealing of the matrices during warm-up was observed to cause sharpening of the atomic lines and some small frequency shifts were also observed.

Table V lists the temperatures at which the absorptions were observed to decrease by 10% in the optical spectra of vanadium atoms isolated in various matrices. These temperatures correlate roughly with *one-third* of the melting point of the respective matrix material and can be considered to be an indication of the temperatures at which V atom bulk diffusion becomes important in these matrices. However, the diffusion properties of the matrix-isolated atoms were found to depend markedly on the deposition conditions. The diffusion temperatures in Table V refer to relatively dilute matrices (V: alkane $\simeq 1{:}10^3$) deposited at 10–12 K.

In most of the alkane matrices, and particularly in the higher alkanes including branched and cyclic isomers, it was possible to observe diminished atomic absorptions at temperatures as high as half of the melting point of the matrix material. Observation of the optical spectra at higher temperatures was complicated by steeply rising baselines and deterioration of matrices caused by slow boil-off and/or detachment from the optical window. Thus a rough limit to the spectroscopically useful working temperature ranges for V atom reactions in these matrices is half of their melting points. Other limits have been suggested[6] and these include the temperature at which the vapor pressure of the matrix material reaches 10^{-3} Torr.

In a recent publication we reported the low-temperature matrix isolation and characterization of diatomic vanadium molecules in noble gas matrices.[4a] Evidence was presented for the formation of these diatomic molecules by diffusion of vanadium atoms on the surface of the matrix during deposition.

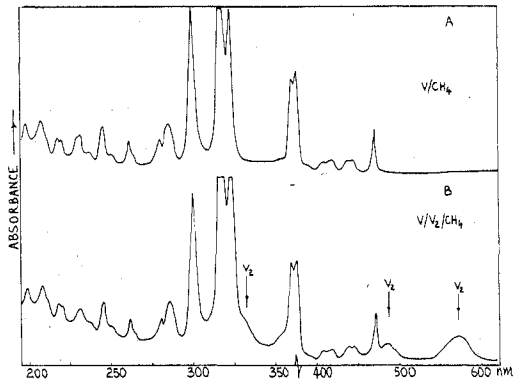

Figure 5. Vanadium concentration study in methane at 10–12 K, (A) $V/CH_4 \simeq 1/10^4$ and (B) $V/CH_4 \simeq 1.5/10^3$, showing the growth of V_2 absorptions at 568 and 486 nm in spectrum B.

Similar quantitative metal deposition studies have been carried out using alkane matrices.

Figure 5 shows a comparison of the optical spectra obtained for vanadium atom depositions in methane matrices at low and at high concentrations. As in $V/V_2/Ar$ matrices (587/494 nm)[4a] two new absorptions are observed in the low-energy region of the spectrum (568/486 nm) obtained for the high metal flux deposition. These new absorptions are believed to be indicative of the presence of diatomic vanadium molecules, and support for this contention has been obtained through quantitative metal deposition studies similar to those previously described for noble gas matrices.[4] A typical log $(A_{V_2}^{568}/A_V^{300})$ vs. log $[R_0]$ plot is shown in Figure 6 (see ref 4 for details) for methane matrices. In addition to the two well-resolved absorption bands attributed to divanadium, two broad partially resolved absorptions near 350 nm may also be noticed in the spectrum obtained for the high metal flux deposition. Although they are poorly resolved, and therefore not susceptible to the analysis performed for the band at 568 nm, these bands are tentatively attributed to divanadium.

The position of the strongest divanadium absorption shows some variation in different matrices. The position of the center of this broad absorption in various matrices is indicated in Table VI. Among the higher alkanes, the position of the absorption shows only small variations. By analogy to the

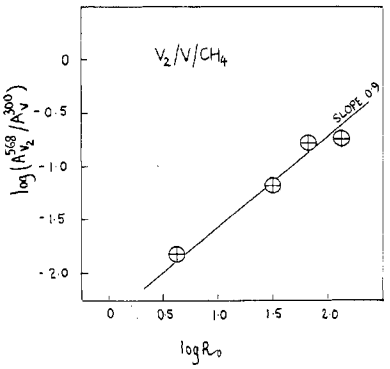

Figure 6. Graphical representation of log $(A_{V_2}{}^{568}/A_V{}^{300})$ vs. log (R_0) for the 568-nm absorption of the new V_n cluster relative to the 300-nm reference absorption of V atoms proving that $n = 2$ (see ref 4 for details of the kinetic analysis).

Table VI. Wavelength Variation of the Strongest Divanadium Absorption in Different Matrices (Units in nm)

Matrix	$\lambda_{max}{}^{V_2}$	Matrix	$\lambda_{max}{}^{V_2}$
Ar	587	n-C_6H_{14}	596
CH_4	568	Cyclohexane	597
C_3H_8	589	2,3-Dimethylbutane	594
n-C_5H_{12}	595	2-Methylpentane	595

discussion of V atomic spectra, we would suggest that these V_2 absorption frequencies in higher alkanes are likely to be closer to the V_2 gas-phase values (which have not yet been reported) than those observed in the lower alkanes and in argon.

The effect of the concentration conditions used during deposition on the degree to which divanadium is formed by diffusion of vanadium atoms in the surface region of argon matrices has been previously reported.[4] In order to assess the influence of alkane matrix materials on the surface diffusion properties of vanadium atoms, a series of experiments has been carried out holding the V metal and gas deposition rates constant and varying only the matrix material. The results for argon, methane, and n-hexane matrices are shown in Figure 7. The order of *decreasing* surface diffusion is seen from Figure 7 to be Ar > CH_4 > n-C_6H_{14}. The relatively low atomic absorptions observed in the case of the argon matrix are indicative of very substantial surface diffusion and clustering of free atoms during deposition. Similar experiments have established the following trend in decreasing surface diffusion: Ar > CH_4 > C_2H_6 > C_3H_8 > C_4H_{10} > C_5H_{12} > C_6H_{14}. It should be noted that the above order applies only for deposition conditions for which the formation of higher clusters, M_n where $n > 2$, may be disregarded. Thus the peak area ratio, V_2/V, was taken as a measure of the extent to which surface diffusion occurred in the various matrices.

The greatest differences in the observed surface diffusion properties are between argon and methane, while relatively small differences are observed among the normal alkanes, as shown in Figure 7. There is, however, a significant trend towards *less* surface diffusion and divanadium formation with increasing chain length of the normal alkane matrix material. A series of experiments employing *different geometrical isomers* of hexane as matrix materials has indicated the following order of decreasing surface diffusion

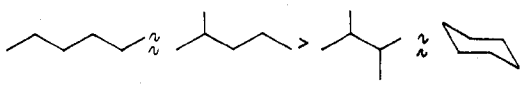

with the V_2/V absorbance ratios falling between ≈0.4 for n-hexane and ≈0.2 for cyclohexane.

An investigation into the factors which determine the influence of the matrix material on the surface diffusion

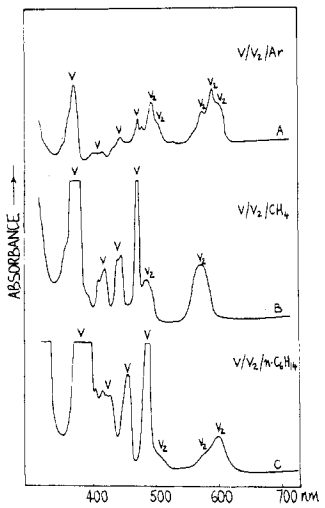

Figure 7. UV–visible spectra of V/matrix ≃ 1.5×10^3 for (A) Ar, (B) CH_4, and (C) n-C_6H_{14} at 10–12 K showing the order of quenching efficiency for V atoms, Ar < CH_4 < n-C_6H_{14}, as measured by A_{V_2}/A_V absorbance ratios.

properties of metal atoms has been carried out in terms of a simple model for the deposition process. The most important feature of this model, which is a steady-state approximation, has been previously described.[4]

A steady-state concentration of the species M, M_2, and M_3 is assumed to exist on the surface of the matrix for a constant metal deposition rate R_0 and a constant gas deposition rate proportional to r. The concentrations of the various species are determined by the following equations

$$dM/dt = R_0 - k_1M^2 - k_2MM_2 - rM = 0$$
$$dM_2/dt = {}^1/_2 k_1M^2 - k_2MM_2 - rM_2 = 0$$
$$dM_3/dt = k_2MM_2 - rM_3 = 0$$

The rate constants k_1 and k_2 refer to the following reactions

$$M \xrightarrow[k_1]{M} M_2 \xrightarrow[k_2]{M} M_3$$

Considering only the formation of diatomic species (as arranged in our alkane experiments), the following relationship may be obtained

$$k_1/r = 2M_2/M^2$$

In terms of this steady-state model, the degree to which dimerization occurs in a given matrix at constant gas and metal deposition rates is related to the rate constant ratio k_1/r, where k_1 is the dimerization rate constant and r is a constant which has been proposed to determine the rate at which the atoms are immobilized in the matrix.[4] For convenience, the quantity r will be referred to as an immobilization rate constant. It should be noted that the dimerization rate constant refers to an *average* rate constant for dimerization throughout the diffusion period. A unique value for the dimerization rate constant is not realistic because of the continuous change toward increasing rigidity which occurs in the environment in which dimerization occurs. If the formation of triatomic and higher polyatomic species is not neglected, then the extent to which metal atom recombination occurs, under given concentration conditions, must be considered in terms of the higher order rate constants, k_2, k_3, etc., and the relative values of these rate constants in different matrices.

In the present study an attempt has been made to quantify the rate constant r in terms of known physical properties of the matrix material. It is assumed that on deposition, the time dependence of the temperature of a thin layer of the matrix is related to the heat of fusion of the matrix material, ΔH_f,

and to parameter C which describes the rate of heat conduction through the matrix. This parameter is related to the thermal conductivity of the matrix material and to the cooling power of the refrigeration unit. An expression for the time dependence of the temperature may be obtained as a solution of the diffusion equation.

$$\partial T/\partial t = D(\partial^2 T/\partial x^2)$$

D ($=K/C_0$) is the thermal diffusivity of the matrix material, where K is the thermal conductivity and C_0 is the heat capacity per unit volume. The solution may readily be shown to be as follows

$$T(x, t) = (Q/(Ct)^{1/2}) \exp(-x^2/4Dt)$$

where $C = C_0 \pi K$ and Q is proportional to ΔH_f the heat of fusion of the matrix material.

Assuming that the time dependence of the temperature is adequately described by the above equation, the rate constant r, for a given matrix material and a constant gas deposition rate, may be related to the heat of fusion of the matrix material, to the parameter C, and to the temperature at which immobilization of the atoms occurs in that matrix, T_0. Substituting ΔH_f for Q, T_0 for T and τ for t the expression for r (where $r = 1/\tau$) in terms of these quantities calculates as follows

$$r = (T_0 - a)^2 C/(\Delta H_f)^2$$

where a is the final temperature of the matrix material. Since the quantity C cannot be evaluated directly, the immobilization rate constants are expressed in a quotient form, r/C. This treatment seems reasonable because the expression for r follows directly from a solution of the diffusion equation. However, the boundary conditions do not fit the problem exactly. The fact that $T \rightarrow \infty$ as $t \rightarrow 0$ is a result of the instantaneous nature of the heat pulse, which is confined to the plane $x = 0$. Also, the instantaneous heat pulse is not really appropriate because of the relatively slow fusion that takes place. In spite of these limitations we feel that the model is useful as a first approximation to obtain at least a qualitative notion of the effect of differing heats of fusion and melting points on the immobilization constant r.

Values of r/C for various matrix materials are tabulated in Table V where the immobilization temperatures, T_0, have been approximated as one-third of the melting point of the respective matrix material.

For two matrix materials for which the rate of heat conduction through the matrix may be assumed to be comparable, i.e., with similar values of the quantity C, the immobilization rate constant ratio r/r' may be obtained from Table V. The ratio r/r' for methane and hexane is thus found to be $r_{CH_4}/r_{C_6H_{14}} = 303/12.0 = 25.2$. This result would favor methane as the more efficient matrix for isolation of atoms over dimers, which is *contrary* to what is observed experimentally. The isolation efficiency is, however, as discussed above, also dependent on the value of the dimerization (diffusion) rate constant. The conclusion is, therefore, that the dimerization rate constant for vanadium atoms in methane is very much greater than that for vanadium atoms in hexane. The general result is that the dimerization rate constants must decrease sharply with increasing chain length of the alkane matrix material. It appears, therefore, that there is a correlation between the magnitude of the dimerization (diffusion) rate constant and the physical size, shape, and molecular weight of the molecules of the normal alkane matrix material. Any further discussion of the relative values of dimerization rate constants is not justified. The reason for this is that the complex nature of the dimerization rate constants, as described above, cannot be taken account of in this simple model.

In the case of the geometrical isomers of hexane, the order of decreasing degree of dimerization follows that which would be expected on the basis of the *relative immobilization rate constants* given in Table V. It would appear, therefore, that for alkanes of similar molecular dimensions, a rough guide to the isolation efficiency of the matrix may be obtained from the relative values of the immobilization rate constants given in Table V. In general, however, differences in dimerization rate constants among the alkanes appear to be much greater than differences in immobilization rate constants, so that the former rate constants exert a stronger influence on the surface diffusion properties in these matrices. The immobilization rate constants tabulated in Table V are therefore not expected to be generally useful in predicting relative isolation efficiencies, since account must also be taken of the dimerization rate constants.

The simple model presented here may not be widely useful in a practical sense, but it provides a basis for discussion of the effects of different matrix materials on the surface diffusion properties of metal atoms in low-temperature matrices. The observed variation of the degree of vanadium atom dimerization among the normal alkane matrices C_nH_{2n+2} (where n = 1–10) has been rationalized in terms of a dependence of the extent of divanadium formation on the relative values of two steady-state rate constants: an immobilization rate constant r, for which relative values may be estimated for matrices of similar thermal conductivity, and a dimerization rate constant k, which appears to decrease with increasing molecular weight and molecular dimensions of the molecules of the alkane matrix material. Comparisons between alkanes and noble gases are more difficult because of differing thermal conductivities, which may be reflected in the immobilization rate constants, and because of other factors such as differences in polarizability, which would be expected to strongly influence the dimerization rate constants.

Conclusion

As different supports become more commonly used in matrix cyrochemical research, it becomes increasingly important to appreciate how these matrices affect the optical spectra of entrapped atoms and the diffusion–aggregation properties of the metal atoms during deposition and subsequent annealing experiments. This information is necessary in order to obtain the fullest information from optical spectra and in order to correctly interpret differences in the optical spectra obtained from different matrices. Besides the spectroscopic subtleties of the research, one would also like to learn how to design specific metal atom syntheses which although kinetically impeded in noble gas supports (4.2–40 K) may well proceed in higher temperature supports (40–300 K). In this way one would also hope to be able to probe the thermal stabilities and reactions of metal atom cocondensation products over an extended temperature range (40–300 K). Particularly intriguing is the possibility of gaining a greater control of the aggregation properties of metal atoms to small, well-defined naked clusters M_n and cluster complexes M_nL_m, for $n > 2$ or 3, than is presently feasible with the noble gases. In future studies we plan to investigate some of the above proposals. An extension of these studies to a greater variety of matrix supports, such as, C_nF_{2n+2}, SF_6, $Si(CH_3)_4$, CO_2, and aromatic hydrocarbons is also desirable.

Acknowledgment. This research was completed while G. A. O. was a Sherman-Fairchild Distinguished Scholar (1977) at California Institute of Technology. The hospitality of the Chemistry Division of Caltech is greatly appreciated. We wish to gratefully acknowledge the financial assistance of the National Research Council of Canada, the Atkinson Foundation, the Connaught Foundation, Imperial Oil of Canada, Erindale College, and the Lash Miller Chemistry Department.

S.M. acknowledges the NRCC for a graduate scholarship.

Registry No. V, 7440-62-2; CH_4, 74-82-8; C_2H_6, 74-84-0; C_3H_8, 74-98-6; C_4H_{10}, 106-97-8; C_5H_{12}, 109-66-0; C_6H_{14}, 110-54-3; C_7H_{16}, 142-82-5; C_8H_{18}, 111-65-9; C_9H_{20}, 111-84-2; $C_{10}H_{22}$, 124-18-5; cyclopentane, 287-92-3; 2-methylbutane, 78-78-4; cyclohexane, 110-82-7; 2-methylpentane, 107-83-5; 2,3-dimethylbutane, 79-29-8; cycloheptane, 291-64-5; 2-methylhexane, 591-76-4; 2,3-dimethylpentane, 565-59-3; cyclopropane, 75-19-4; cyclooctane, 292-64-8; Ar, 7440-37-1.

References and Notes

(1) (a) D. Gruen in "Cryochemistry", M. Moskovits and G. A. Ozin, Ed., Wiley, New York, N.Y., 1976; (b) D. M. Mann and H. P. Broida, *J. Chem. Phys.*, **55**, 84 (1971); (c) W. Klotzbücher and G. A. Ozin, *Inorg. Chem.*, **15**, 292 (1975); (d) O. M. Kolb, D. Leutloff, and W. Schulze, *J. Chem. Phys.*, **66**, 2806 (1977), and references cited therein.
(2) (a) J. D. McCullough and W. W. Duley, *Spectrosc. Lett.*, **8**, 51 (1975); (b) W. R. M. Graham and W. W. Duley, *J. Chem. Phys.*, **55**, 2527 (1971).
(3) (a) K. J. Klabunde, H. F. Efner, T. O. Murdock, and R. Ropple, *J. Am. Chem. Soc.*, **98**, 1021 (1976); (b) K. J. Klabunde, H. F. Efner, L. Satek, and W. Duley, *J. Organomet. Chem.*, **71**, 309 (1974).
(4) (a) T. A. Ford, H. Huber, W. Klotzbücher, E. P. Kündig, M. Moskovits, and G. A. Ozin, *J. Chem. Phys.*, **66**, 524 (1977); (b) M. Moskovits and J. Hulse, *J. Chem. Soc., Faraday Trans. 2*, 471 (1977).
(5) M. Moskovits and G. A. Ozin, *Appl. Spectrosc.*, **26**, 481 (1972); E. P. Kündig, M. Moskovits, and G. A. Ozin, *J. Mol. Struct.*, **14**, 137 (1972).
(6) H. E. Hallam and G. F. Scrimshaw in "Vibrational Spectroscopy of Trapped Species", H. E. Hallam, Ed., Wiley-Interscience, New York, N.Y., 1973, Chapter 2.
(7) D. H. W. Carstens, W. Braschear, O. R. Eslinger, and D. M. Gruen, *Appl. Spectrosc.*, **26**, 184 (1972).

Contribution from the Lash Miller Chemistry Laboratories and Erindale College, The University of Toronto, Toronto, Ontario, Canada

Cryochemical Studies of Zerovalent Copper–Ethylene Complexes, $(C_2H_4)_nCu$ and $(C_2H_4)_mCu_2$ (Where n = 1–3; m = 4 or 6), and Their Use in Forming Copper Clusters. Localized Bonding Models for Ethylene Chemisorption onto Bulk Copper

GEOFFREY A. OZIN,* HELMUT HUBER, and DOUGLAS McINTOSH

Received June 1, 1977 AIC70395K

Cryochemical reactions of copper atoms with ethylene and ethylene/argon mixtures at 10–12 K using copper concentration conditions which favor *mononuclear* reaction products give rise to a series of three, highly colored, binary copper–ethylene complexes. Vibrational and electronic spectroscopy taken in conjunction with copper/ethylene/argon concentration experiments, $^{12}C_2H_4/^{13}C_2H_4$/Ar mixed isotope substitution studies, and comparisons with $(C_2H_4)_nCo$ and $(C_2H_4)_nNi$ (where n = 1–3) provide strong evidence in support of a similar $(C_2H_4)_nCu$ formulation. Particularly noteworthy properties of these copper–ethylene complexes concern their marked *instability* relative to their respective nickel complexes, although this is thought to be partly a manifestation of their paramagnetic character and tendency toward dimerization. Electronically, the $(C_2H_4)_nCu$ complexes comprise a unique series in that they *all* display intense *visible* and *ultraviolet* charge-transfer absorptions which monotonically *red* and *blue* shift respectively with increasing ethylene stoichiometry. These spectral trends when taken together with the available electronic spectral data for copper(I)–ethylene complexes as well as the results of semiempirical molecular orbital calculations for $(C_2H_4)_nCu$ allow a reasonable assignment of the visible and ultraviolet charge-transfer bands to be made. Quantitative Cu/C_2H_4 concentration experiments and controlled annealing (30–45 K) of matrices containing $(C_2H_4)_nCu$ (where n = 2, 3) provide convincing evidence for a transformation to $(C_2H_4)_mCu_2$ (where m = 4 or 6). Especially interesting is the observation that thermal annealing of $(C_2H_4)_mCu_2$ in the higher temperature range 45–100 K seems to present a route to small, copper clusters. Finally, the value of these mononuclear and binuclear copper–ethylene complexes as localized bonding representations for ethylene chemisorbed onto bulk copper is briefly contemplated in the light of recent ultraviolet photoemission spectra for ethylene chemisorbed onto copper surfaces.

Introduction

While it is true that a wide variety of copper(I)–olefin complexes are known,[1] some of which are catalysts for photochemical reactions of alkenes,[2] there are no known examples of room temperature, stable, zerovalent copper–olefin complexes. One must presume that this is a manifestation of the weakness of copper(0)–olefin interactions and in a localized bonding sense[3] mirrors the poor chemisorptive capacity of bulk copper for alkenes at room temperature.[4] In this paper we report synthetic, vibrational, and electronic information for $(C_2H_4)_nCu$ and $(C_2H_4)_mCu_2$ (where n = 1–3; m = 4 or 6) noting that a brief report of the mononuclear complexes has already been presented.[5] The use of these complexes as "chemisorption models" for ethylene bonded to copper surfaces,[3,4] as well as an interesting new source of small copper clusters,[25] is carefully assessed.

Experimental Section

Monatomic copper was generated by directly heating a thin tungsten rod (0.025 in.) around the center of which was wound copper wire (0.005 in.). The copper metal (99.99%) was supplied by McKay, New York, N.Y., Research grade $^{12}C_2H_4$ (99.90%) was supplied by Matheson of Canada and $^{13}C_2H_4$ (95%) by Stohler Isotopes, Montreal. The furnace used for the evaporation of the metals has been described previously.[6] The rate of copper atom deposition was continuously monitored using a quartz crystal microbalance.[6] In the infrared experiments, matrices were deposited on either a NaCl or CsI plate cooled to 10 K by means of an Air Products Displex closed cycle helium refrigerator. Infrared spectra were recorded on a Perkin-Elmer 180 spectrophotometer. Ultraviolet–visible spectra were recorded on a standard Varian Techtron instrument in the range 190–900 nm, the sample being deposited on a NaCl optical plate. Extended Hückel molecular orbital calculations were run on an IBM 370 computer.

Results and Discussion

In a preliminary report[5] we recently communicated the observation that the reaction between copper atoms and ethylene at 10–12 K leads not only to monoethylene copper $(C_2H_4)Cu$ (**13e**) but also to $(C_2H_4)_2Cu$ (**15e**) (which at the time represented the first example of a binary bis(ethylene) transition-metal complex) and $(C_2H_4)_3Cu$ (**17e**), which can be considered to be the next highest member of the series $(C_2H_4)_3Co$ (**15e**),[7] $(C_2H_4)_3Ni$ (**16e**).[8] However, these conclusions were based only on copper/ethylene/argon concentration studies as monitored by matrix infrared spectroscopy.[5]